IOP Publishing Modelling and Simulation in Materials Science and Engineering

Modelling Simul. Mater. Sci. Eng. **32** (2024) 065008 (16pp) https://doi.org/10.1088/1361-651X/ad585e

The property of $CrCoNiFeMnAl_x$ (x=0, 0.5, and 1) high-entropy alloys on rapid cooling: insights from *ab initio* molecular dynamics

Luyu Wang[1,*], Xinxin Liu[2] and Zhibin Gao[3,*]

[1] College of Artificial Intelligence and E-Commerce, Zhejiang Gongshang University Hangzhou College of Commerce, Hangzhou 311599, People's Republic of China
[2] Department of Materials Science and Engineering, University of Pennsylvania, Pennsylvania 19104, United States of America
[3] State Key Laboratory for Mechanical Behavior of Materials, Xi'an Jiaotong University, Xi'an 710049, People's Republic of China

E-mail: Dr.luyu-wang@hotmail.com and zhibin.gao@xjtu.edu.cn

Received 21 March 2024; revised 2 June 2024
Accepted for publication 14 June 2024
Published 25 June 2024

Abstract

High-entropy alloys (HEAs) are currently the subject of extensive research. Despite this, the effects of rapid cooling on their performance have yet to be investigated. This study uses *ab initio* molecular dynamics to investigate the $CrCoFeNiMnAl_x$ ($x = 0$, 0.5 and 1) HEAs under a rapid cooling process. It has been observed that the three HEAs all form metallic glass at 300 K under a constant cooling rate of 1.25×10^2 K ps^{-1}, mainly composed of icosahedron and face-centered cubic clusters. Secondly, the glass transition temperatures (T_g) are predicted to be 1658 K for CrCoFeNiMn, 1667 K for $CrCoFeNiMnAl_{0.5}$, and 1687 K for CrCoFeNiMnAl, respectively. It can be seen the T_g of HEAs increases with the content of Al increasing. Eventually, a relationship between structure and dynamics is established by using the five-fold local symmetry parameters and shear viscosity, which proves that structural evolution is the fundamental reason for dynamic deceleration. The present results contribute to understanding the evolution of the local structure of $CrCoFeNiMnAl_x$ and provide a new perspective for studying the structural mechanism of dynamic retardation in HEAs.

Keywords: *ab initio* molecular dynamics, structural evolution, dynamical property, high-entropy alloys, metallic glass

* Authors to whom any correspondence should be addressed.

1. Introduction

The high-entropy alloy (HEA) is first proposed and named by Yeh *et al* [1] in 2004 and can generally be defined as new materials with 5 or more elements, each element accounting for between 5% and 35% of the total atomic number [2, 3]. Unlike the traditional alloys, which tend to undergo material embrittlement with metal type increasing, the composition of HEA is complex, and the atoms of constituent elements are randomly and disordered in the lattice positions, leading to the HEA with a high entropy effect in thermodynamics, slow diffusion effect in dynamics, lattice distortion effect in structure and cocktail effect in performance [4]. The mixing entropy of the material greater than 1.6 R (R is a gas constant) results from this novel mixing mode which reduces the Gibbs free energy of the material, inhibits the formation of intermetallic compounds and intermediate equal complex phases, and tends to form disordered solid solutions, such as face-centered cubic (FCC), body-centered cubic (BCC), and hexagonal close-packed structure [5]. It is also found that each principal element in HEA affects the overall properties of the alloy together, and shows its characteristics and compound effects through the interaction of alloying elements as well. For instance, Wang *et al* [6] added Al element to CoCrCuFeNi HEA and found that it could improve the oxidation resistance of the HEA at high temperatures and promote the formation of the BCC phase, leading to the improvement of strength. Further, amorphous structures may be precipitated in the HEA, which can significantly improve its mechanical properties in terms of solid solution strengthening, precipitation strengthening, and nano/amorphous composite strengthening. Currently, there are two ways to obtain amorphous structures. One is to destabilize the crystalline solid phase into a disordered solid phase, such as stretching [7]. However, this amorphization only occurs in localized dislocation areas, such as crack tip fields. Rapid cooling of metal melts is another major route of amorphization, which maintains dynamic disorder in the liquid phase of the rapidly cooled liquid phase and can be used to produce bulk amorphous alloys [8]. Therefore, amorphization CrCoFeNiMnAl may have excellent properties that traditional materials cannot match, such as outstanding performance in mechanics, electromagnetism, high-temperature resistance, and corrosion resistance, so it is regarded as one of the key candidate materials that are expected to solve the bottleneck problems of material performance in the current engineering field

Although the influence of Al content on CrCoFeNiMn HEA has been explored widely by experiments, the properties of liquid and amorphous HEAs have not been explicitly studied [9–11]. The properties of the liquid phase, especially transport and thermodynamic properties, play an important role in understanding and predicting the microstructure evolution model of HEAs during solidification. These liquid local structures also provide very important benchmark results for the development of the classical force field model. Additionally, after fast cooling, the multi-component metal melt will maintain an amorphous phase, namely metallic glass. It not only has the advantages of metal and glass, but also overcomes their respective disadvantages, such as higher strength than steel, higher hardness than high hardness tool steel, and equipping certain toughness and rigidity. Despite the importance of liquid and amorphous properties, their experimental measurement in high-temperature melts and rapid cooling is challenging, and AIMD simulations have emerged as a powerful framework for studying HEAs. In this study, AIMD simulations are conducted to investigate three kinds of HEAs with chemical compositions of CrCoFeNiMn, $CrCoFeNiMnAl_{0.5}$, and CrCoFeNiMnAl, respectively, to comprehensively explore the effect of Al content on the solidification process of $CrCoFeNiMnAl_x$.

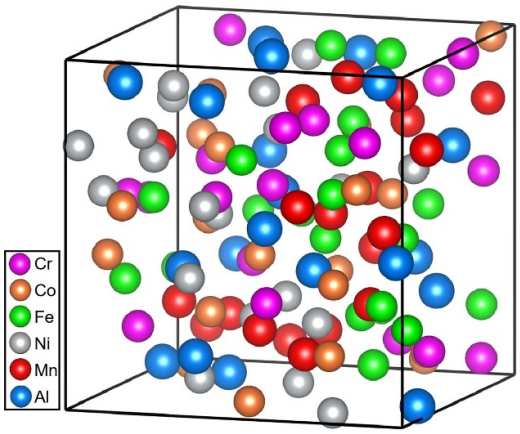

Figure 1. The structural model of CrCoFeNiMnAl HEA.

2. Methodology

AIMD simulations of CrCoFeNiMn, CrCoFeNiMn$Al_{0.5}$, and CrCoFeNiMnAl alloys are implemented by the Vienna Ab-Initio Simulation Package [12–14]. The exchange-correction energy of the electrons is treated by the generalized gradient approximation in the form of Perdew–Burke–Ernzerhof functional [15, 16]. The electron-ion interaction is approximated by Projector-Augmented-Wave pseudopotentials [17, 18]. The wave function of valent electrons is expanded in plane wave basis set with an energy cutoff of 400 eV and the energy convergence criterion of the electronic self-consistency is set to 10^{-6} eV per atom [19]. Newton's equation of motion is solved through Verlet's algorithm with a time step of 3 fs. The spin polarization is utilized in the simulation because elements Cr, Co, Fe, Ni, and Mn have unpaired electrons in their valent shells.

The simulated CrCoFeNiMn alloy is composed of 20 Cr, 20 Co, 20 Fe, 20 Ni, and 20 Mn with a molar percentage of 20% for each element [20, 21]. For the CrCoFeNiMn$Al_{0.5}$ alloy, ten extra Al atoms are added to the CrCoFeNiMn alloy with 9.09 at% of Al; For the CrCoFeNiMnAl alloy (figure 1), 20 Al atoms are added with the concentration of Al at 16.67 at%. Only Γ point is considered to sample the supercell Brillouin zone. All dynamical simulations are performed in the NVT (*i.e.* constant atom number, volume, and temperature) ensemble by means of a Nosé–Hoover thermostat to control temperature. The equation of motion is solved through Verlet's algorithm with a time step of 3 fs. To avoid the memory effect from the initial random structure, the initial configurations are heated to 3000 K, taking CrCoFeNiMnAl alloy as an example, as shown in figure 1, and then step-wise cooled down to 2700, 2400, 2100, 1800, 1500, 1200, 900, 600, and 300 K at constant cooling rates of 1.25×10^2 K ps^{-1}. After quenching down to the desired temperature, the equilibrium volume of supercells is obtained by adjusting the internal pressure close to 0 [22]. At each target temperature, the equilibrium volume is used as input configuration in the following 10 000 steps of NVT ensemble simulation [23–26]. The first 6000 steps are used to relax the system to reach thermal equilibrium and the remaining 4000 AIMD steps are used for the analysis of the structure and kinetic properties.

The simulated densities of the studied systems can be obtained from the equilibrium volume. At 300 K, the simulated densities of CrCoFeNiMn, CrCoFeNiMn$Al_{0.5}$, and

CrCoFeNiMnAl are 8.23, 7.63, and 7.22 g cm^{-3}, respectively. Li *et al* [27] measured the density of CrCoFeNiMn manufactured by selective laser melting technology is about 7.9 g cm^{-3}. The error between this value and the simulated density of 8.23 g cm^{-3} is within a reasonable range with an absolute deviation of about 4.18%. From the analysis, the structural optimization method in this study provides a satisfactory volume.

3. Results and discussions

3.1. Radial distribution function

The radial distribution function (RDF) is a pair correlation that expresses the probability of finding atoms as a function of distance r from an average center atom. The structure information is reflected by the peak position, peak shape, intensity, etc. Typically, the atoms in the nearest-neighbor shell, contributing to the first peak in RDF, form a short-range ordered structure. The partial RDF of atom pair *i–j* is defined as follows [28],

$$g_{ij}(r) = \frac{V}{N_i N_j} \left\langle \sum_{\alpha=1}^{N_i} \frac{n_{\alpha j}(r,\ \Delta r)}{4\pi r^2 \Delta r} \right\rangle \tag{1}$$

where V is the volume of the supercell, i is the central atom, j is the coordination atom, N_i and N_j are the numbers of i and j atom in the supercell, respectively, $n_{\alpha j}(r, \Delta r)$ is the number of j species in the sphere shell from r to $r + \Delta r$, and the symbol $\langle \cdots \rangle$ represents the time average.

Figure 2 exhibits the total radial distribution function (TRDF) of three HEAs as a function of temperature and the partial radial distribution function (PRDF) of CrCoFeNiMn melts at 1800 K. From figure 2(d), it is obvious that the intensity of the first peak is different, especially the Cr–Cr pair, which has the lowest intensity but the widest spectrum compared with all other pairs. Except for the first peak, the PRDFs of all pairs almost overlap. These two phenomena are consistent with research results from Ding *et al* [29]. In addition, from table 1, the positions of the three peaks of TRDFs for three HEAs are situated at 2.40–2.46, 4.07–4.18, and 4.75–4.83 Å at 300 K, respectively. In comparison, previous studies by Jiang *et al* [30] and Li *et al* [31] using molecular dynamics simulations have reported the three peak positions of Al_xCoCrFeNi at about 2.5, 4.25, and 5.0 Å and for AlCoCrCuFeNi at approximately 2.5, 4.18, and 4.90 Å at same temperature. Given the absence of available experimental data for the investigated systems, we compare our results only to those from molecular dynamics simulations of similar systems. While these comparisons are not strictly rigorous, they do provide reasonable support for our FPMD simulations. Therefore, we explore the AIMD method to predict the typical local structures evolution and dynamics properties of the three HEAs.

Figures 2(a)–(c) show that in the temperature range of 3000–1800 K, all TRDFs display an intense first peak, a distinct second peak, and a weak third peak, which is the common behavior of liquid at high temperatures. The amplitude of these peaks gradually increases with the decrease of temperature, indicating that the degree of the dense and ordered arrangement of atoms is enhanced. In addition, with the decrease of temperature, the position of the first peak gradually moves to the right. At 1500 K, the second peak tends to split into two sub-peaks, and the third peak suddenly becomes strong, meaning that the HEAs are on the eve of phase transformation. As the temperature decreases from 1200 to 300 K, the second peak of all TRDFs splits into two sub-peaks, and the sub-peak on the left is slightly higher than the right one, which is an indicator of amorphous transformation. Zhang *et al* [32] and Liu *et al* [33] reported that the R_i/R_1 (R_i is the ith peak position) of liquids and glasses has a universal scaling behavior, that is, the R_1/R_1 and R_2/R_1 of all liquids are about 1.00 and 1.86, while the R_i/R_1

Table 1. The first peak position R_1 (Å) of TRDFs and ratios R_i/R_1 for liquid and the obtained solid glass under the constant cooling rate.

System	T (K)	R_1	R_1/R_1	R_2/R_1	R_3/R_1	R_4/R_1	R_5/R_1
CrCoFeNiMn	300	2.40	1.00	1.74	1.98	2.59	3.45
	1800	2.37	1.00	1.84	2.68	3.53	
$CrCoFeNiMnAl_{0.5}$	300	2.44	1.00	1.67	1.98	2.54	3.46
	1800	2.38	1.00	1.86	2.70	3.54	
CrCoFeNiMnAl	300	2.46	1.00	1.67	1.96	2.52	3.43
	1800	2.42	1.00	1.79	2.67	3.60	
SPO theory			1.00	1.80	2.60	3.40	
Statistical value			1.00	1.73	2.00	2.64	3.45

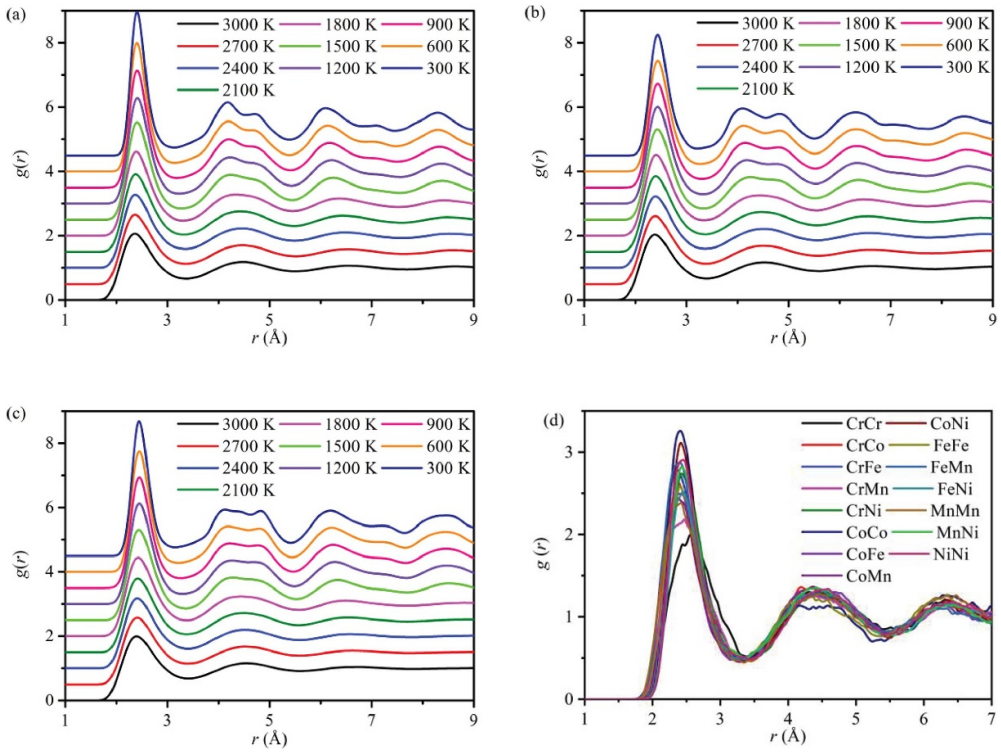

Figure 2. The temperature evolution of TRDFs of (a) CrCoFeNiMn, (b) $CrCoFeNiMnAl_{0.5}$, and CrCoFeNiMnAl (c). For clarity, each curve is vertically displaced from the curve below. (d) is PRDFs of CrCoFeNiMn melt at 1800 K. (*Note* that, for clarity, each curve has been vertically displaced from the curve below.).

($i = 1, 2..5$) for all metallic glasses are close to standard values: $\sqrt{1}(1.00)$, $\sqrt{3}(1.73)$, $\sqrt{4}(2.00)$, $\sqrt{7}(2.64)$, and $\sqrt{12}(3.46)$ [32]. A statistical analysis of the RDF, normalizing all the peak positions R_i ($i = 1, 2\ldots5$) to R_1, is executed to further research the structural characteristics of the HEAs under a constant cooling rate, 1.25×10^2 K ps^{-1}. The ratios of R_i/R_1 ($i = 1$–4 for

undercooled liquid at 1800 K and i = 1–5 for solid glass at 300 K) in TRDFs are calculated and listed in table 1. It can be found that the R_i/R_1 of three HEAs at 1800 K is about 1.00, 1.83, 2.68, and 3.56, consistent with the values (1.0, 1.80, 2.60, and 3.40) originated from spherical-periodic order (SPO) theory, which means that the arrangement of atoms in the HEAs undercooled melt can be well described by the SPO theory. At 300 K, the values of R_i/R_1 (i = 1–5) are approximately 1.00, 1.74, 1.98, 2.59, and 3.45, respectively. These ratios of R_i/R_1 (i = 1–5) are almost the same as $\sqrt{1}$, $\sqrt{3}$, $\sqrt{4}$, $\sqrt{7}$, and $\sqrt{12}$, suggesting that under such a cooling rate, the three HEAs form amorphous structure, named metal glass. However, it is worth mentioning that the difference of R_i/R_1 (i = 3 and 4) between solid glass and undercooled liquid is significant, which is related to the local translational symmetry. To sum up, the global atomic packing in the CrCoFeNiMnAl$_x$ HEAs can be described by the combination of SPO and local translational symmetry.

3.2. Voronoi tessellation analysis

Due to the limitation of statistically average RDFs in the three-dimensional structure information, the Voronoi tessellation method is employed to further explore the short-range arrangement of atoms. The Voronoi polyhedron (VP) is represented by Schläfli's notation, $\langle n_3, n_4, n_5, n_6\rangle$, where n_i is the number of faces with i vertices. The Voronoi indices of standard BCC, FCC, and ICOS are $\langle 0, 6, 0, 8\rangle$, $\langle 0, 12, 0, 0\rangle$, and $\langle 0, 0, 12, 0\rangle$, respectively [32].

It has been previously reported that the preference for polyhedrons depends on the effective atomic radius ratio (R^*) between the solute and solvent. With the reduction of R^*, the preferred polyhedron change from a Frank–Kasper polyhedron ($R^* > 1.2$) to an icosahedron ($R^* < 0.902$), and then to a bi-capped square Archimedean antiprism polyhedron ($R^* < 0.835$), and finally to a tricapped trigonal prism packing type polyhedron ($R^* < 0.732$) [34]. In this study, since the proportion of each element in the high entropy alloy is similar, each element can be a solvent or solute. Consequently, according to the Goldschmidt radii, the R^* is between 0.87 (Ni/Al) to 1.15 (Al/Ni), predicting icosahedral dominance in HEAs melt. The top 18 Voronoi indices of three HEAs at four representative temperatures (300, 1500, 1800, and 3000 K) are displayed in figure 3. During the cooling process, the clusters in the three HEAs all tend to form polyhedrons with Voronoi indices of <0, 3, 6, 4>, <0, 3, 6, 5>, <0, 4, 4, 6>, <0, 0, 12, 0>, <0, 2, 8, 2>, <0, 2, 8, 4>, <0, 2, 8, 5>, <0, 1, 10, 2>, <0, 1, 10, 3>, <0, 3, 6, 6>, <1, 2, 6, 3, 1>, <1, 3, 5, 4, 1>, and <1, 3, 4, 5, 2>. Although there are numerous kinds of VPs, polyhedron <0, 3, 6, 4>, <0, 2, 8, 4>, and <0, 1, 10, 2> always occupies a relatively large proportion during the whole cooling process.

To clarify the structural evolution of three HEAs in detail, these preferred polyhedra are classified into four categories [35]: (a) <0, 3, 6, 4>, <0, 3, 6, 5>, <0, 4, 4, 6>, and <0, 4, 4, 7> are considered to be FCC-like clusters; (b) <0, 6, 0, 8> represents BCC-like clusters; (c) <0, 0, 12, 0>, <0, 1, 10, x>, <0, 3, 6, 3>, <0, 2, 8, x> (x = 1, 2…6), and <1, 0, 3, 9> represent ICOS-like clusters; (d) the remaining Voronoi indices are unknown structures. Based on the rule, it is obvious that the ICOS-like and FCC-like clusters have been already populated in the three HEAs because of the cluster <0, 3, 6, 4>, <0, 3, 6, 5>, <0, 4, 4, 6>, <0, 2, 8, 2>, <0, 2, 8, 4>, and <0, 1, 10, 2> existing in both liquid and glassy state. Furthermore, the variation of ICOS-like and FCC-like clusters with the decrease in temperature is plotted in figure 3(d). In the temperature range of 3000–1800 K, that is alloy melt, the fraction of ICOS-like and FCC-like clusters varies between 8.19%–23.71% and 6.15%–11.87% for CrCoFeNiMn, 7.87%–22.15% and 5.87%–10.71% for CrCoFeNiMnAl$_{0.5}$, and 7.26%–20.03% and 5.40%–10.88% for CrCoFeNiMnAl, validating above hypothesis that icosahedral dominates in HEAs melt. At 1500 K, the amount of ICOS-like clusters in the three HEAs rises drastically by over

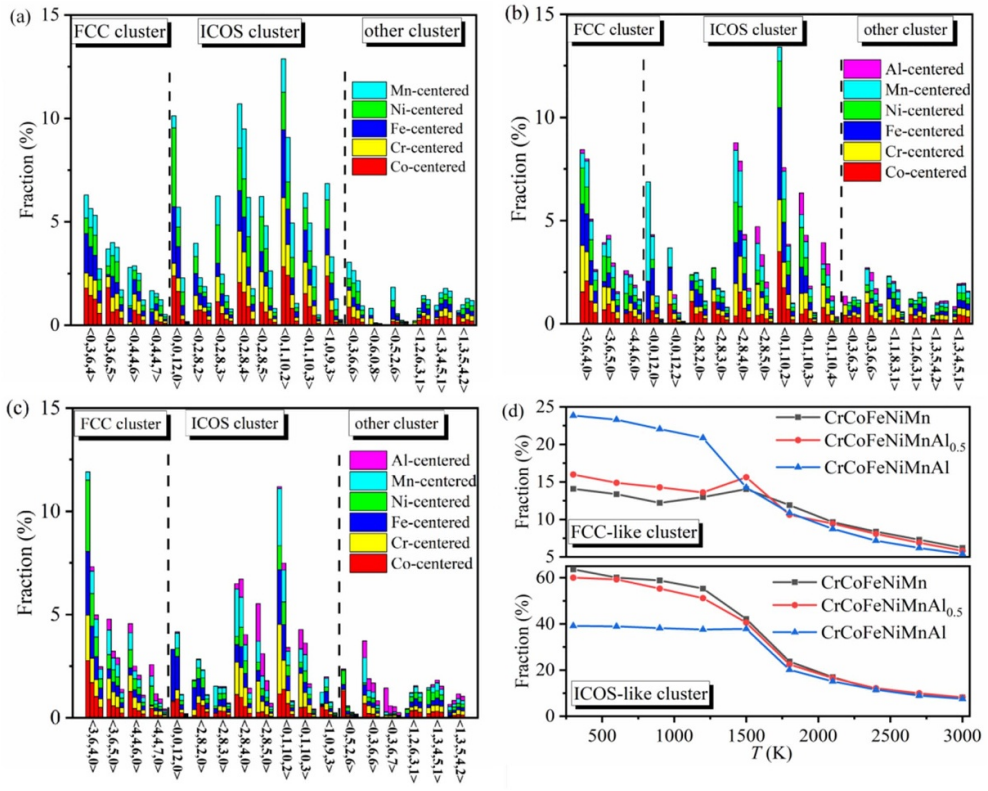

Figure 3. Fraction of main Voronoi indices in CrCoFeNiMn (a), $CrCoFeNiMnAl_{0.5}$ (b), and CrCoFeNiMnAl (c) melts at four temperatures, from left to right, they are 300, 1500, 1800, and 3000 K, and the fraction of ICOS-like and FCC-like clusters versus temperature (d).

80% and that of FCC-like clusters normally raises about 20%, which is achieved by depleting various low population VP types with low symmetry. This means that compared with high-temperature melts, the atomic structure at this temperature becomes heterogeneous, and the increase of these clusters leads to the first peak of the RDF curve becoming sharper with the decrease in temperature. As the temperature drops from 1200 to 300 K, the percentage of ICOS-like clusters continues to increase. At 300 K, the ICOS-like cluster and FCC-like cluster of CrCoFeNiMn are 63.62% and 14.08%, that of $CrCoFeNiMnAl_{0.5}$ is 59.95%and 16.01%, and that of CrCoFeNiMnAl is 39.07% and 23.83%. Correspondingly, the ratio of ICOS-like cluster to FCC-like cluster is 4.52, 3.74, and 1.64, respectively. The different ratios lead to different shapes of the second peak of RDFs.

3.3. Five-fold symmetry parameter

From the above discussion, we know that these three HEAs undergo phase transformation during rapid solidification, from the liquid state at 1800 K to the glass state at 1500 K. To determine the glass transition temperature of HEAs under the cooling rate of 1.25×10^2 K ps^{-1}, a five-fold symmetry parameter W is introduced and defined as, [36–38]

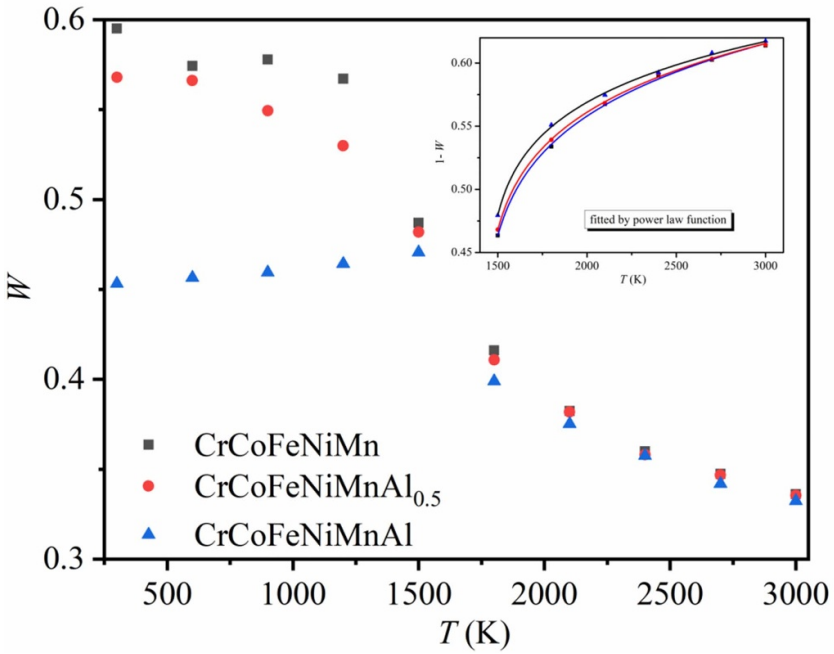

Figure 4. Temperature dependence of W for the three HEAs. The inset shows the power law relationship between W and T.

$$W = \sum_i \left(f_i^5 \times P_i\right) \tag{2}$$

where P_i is the percentage of polyhedron type i, and f_i^5 is the percentage of the 5-edged polygon in the VP and evaluated as follows,

$$f_i^5 = \frac{n_i^5}{\sum_{k=3,4,5,6} n_i^k} \tag{3}$$

in which n_i^k is the number of k-edged polygons in VP type i. The W of three HEAs as a function of temperature is revealed in figure 4. It can be seen that the W values of the three HEAs increase with decreasing temperature, grow sharply between 1800 and 1500 K, and lightly raise for CrCoFeNiMn, slightly decrease for CrCoFeNiMnAl, and continuously increase for $CrCoFeNiMnAl_{0.5}$ after 1500 K. Furthermore, in the temperature range of 3000–1500 K, the change of W with temperature seems to follow some functional relationship. The power law of $(1–W) \sim (T–T_1)^{\alpha}$ is employed to fit W as a function of temperature. As shown in the illustration in figure 4, the simulated data are fitted well with the power law function, and the statistical correlation parameter R^2 is better than 0.99. The fitted values of T_1 are 1409 K for CrCoFeNiMn, 1417 K for $CrCoFeNiMnAl_{0.5}$, and 1434 K for CrCoFeNiMnAl. Parisi and Sciortino [39] reported that T_1 was approximately equal to 0.85 T_g (T_g is the ideal glass transition temperature). Consequently, the values of T_g are 1658 K for CrCoFeNiMn, 1667 K for $CrCoFeNiMnAl_{0.5}$, and 1687 K for CrCoFeNiMnAl, respectively. A conclusion can be drawn that with the increase of Al, the glass transition temperature (T_g) of HEAs increases.

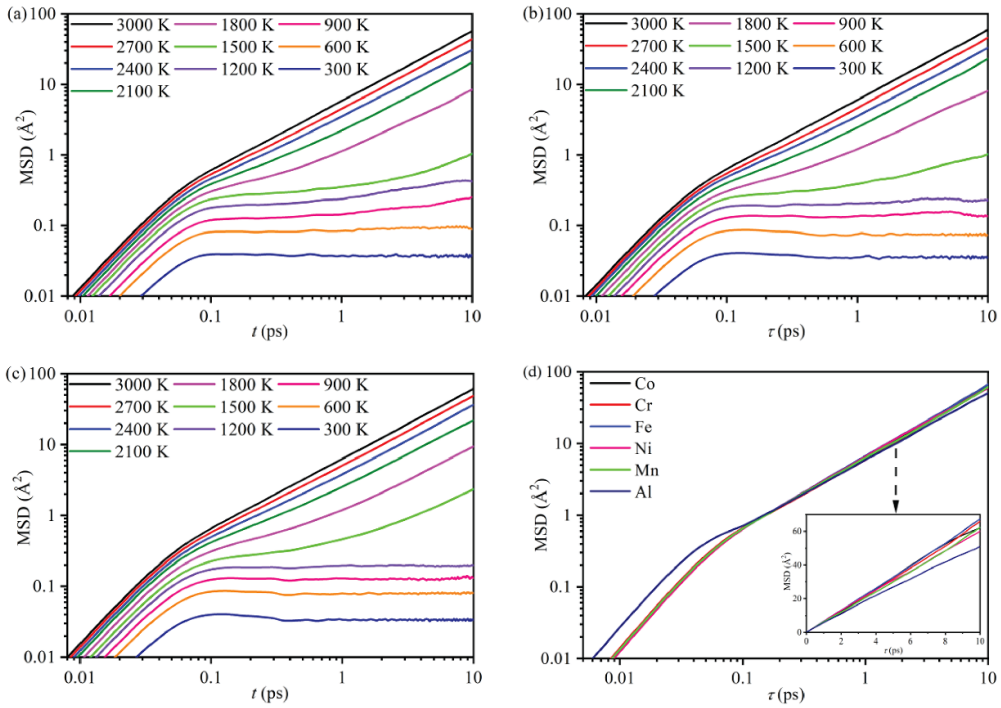

Figure 5. The total MSD of (a) CrCoFeNiMn, (b) CrCoFeNiMnAl$_{0.5}$, and (c) CrCoFeNiMnAl as a function of time at multiple temperatures and (d) the partial MSD of each element in CrCoFeNiMnAl liquid at 1800 K.

3.4. Self-diffusion coefficients and dynamic susceptibility

The dynamic characteristics is another important information for a comprehensive understanding of alloy properties. For this, the mean square displacement (MSD) as a function of time is often used to the dynamic motion of atoms and is defined as,

$$R_{i\alpha}^{2}(t) = \frac{1}{N_\alpha}\left\langle \sum_{i=1}^{N_\alpha} \left| R_{i\alpha}(t+\tau) - R_{i\alpha}(\tau) \right|^2 \right\rangle \tag{4}$$

where N_α is the total atomic number of species α, $R_{i\alpha}$ is the coordinates of atom i, and τ is the arbitrary origin of time. Figure 5 shows the total MSD of three HEAs at various temperatures and the MSD of each element in CrCoFeNiMnAl alloy at 1800 K. In this case, the atomic motion of the three HEAs can be divided into three parts: (i) In a very short time in the beginning, owing to the ballistic motion of atoms, all MSD curves grow in a quadratic form with the increase of relaxation time. During this period, the growth rate of the total MSD curve slightly increases with the increase of Al content. This is because the ballistic motion is related to the atomic mass. The smaller the mass, the faster the speed, as shown in figure 5(d). Therefore, adding an Al element with a small relative atomic mass can improve the growth rate of the total MSD curve. (ii) In the intermediate period, at high temperature, the intersection with the linear diffusion region can be detected after ballistic growth, while at low temperature, a plateau appears on the MSD curve and becomes more obvious with the temperature decreasing because of the so-called 'cage effect'. Each atom is surrounded by an effective cage formed by

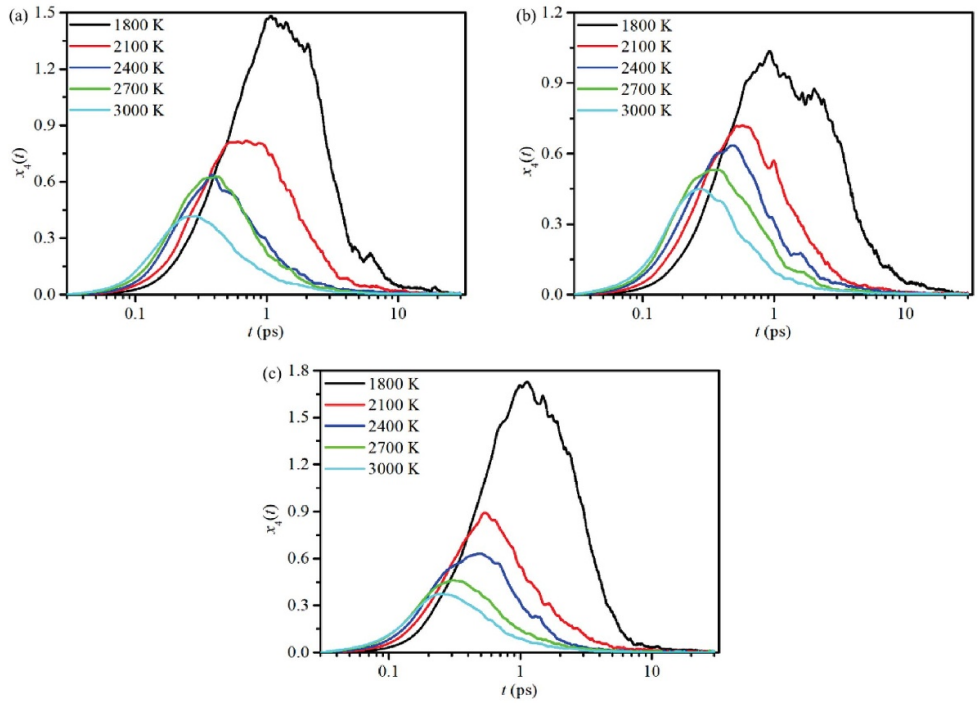

Figure 6. The dynamic susceptibility of (a) CrCoFeNiMn, (b) CrCoFeNiMnAl$_{0.5}$, and (c) CrCoFeNiMnAl as a function of time from 3000 to 1800 K.

adjacent atoms, which limits the movement of the atom within a range close to its original position. From the figures 5(a)–(c), it can be found that the MSD curves of three HEAs show a clear plateau at $T \leqslant 1500$ K, which is an indicator of β-relaxation. This shows that the relaxation time of different atoms in the whole system is different, and they have a distribution in space. In other words, the system presents dynamic heterogeneity [39]. (iii) $T \geqslant 2100$ K, the atoms successfully escape the cage after a long enough time, resulting in a diffusive motion with a linear dependence of MSD on time. However, $T \leqslant 1200$ K, even after a sufficiently long time, the MSD oscillates around a mean value, which implies that the atoms cannot run away from the cage and are confined to the vicinity of the original position, with only thermal vibration. The oscillating MSD curves also confirm that HEAs have solidified at these temperatures.

From the MSD analysis, the dynamic heterogeneity of the HEAs melts at 1800 K is not distinct. To clarify this point, the dynamic susceptibility ($\chi_4(t)$) is calculated from the atomic motion trajectory, which is obtained by the following equation [40],

$$\chi_4(t) = N^{-1}\left(Q(t)^2 - \langle Q(t)\rangle^2\right) \tag{5}$$

where the $Q(t)$ is the overlap function. The dynamic susceptibility of three HEAs from 3000 to 1800 K are shown in figure 6. $\chi_4(t)$ approaches 0 in a very short time, and then reaches a peak with the increase of time. If the time increases further, it will continue to decay to 0. This is because the dynamic non-uniformity is most obvious in the middle of time. More importantly, as the temperature decreases, the peak value of $\chi_4(t)$ will increase, and the time corresponding to the peak value will also increase. This shows that the degree of dynamic

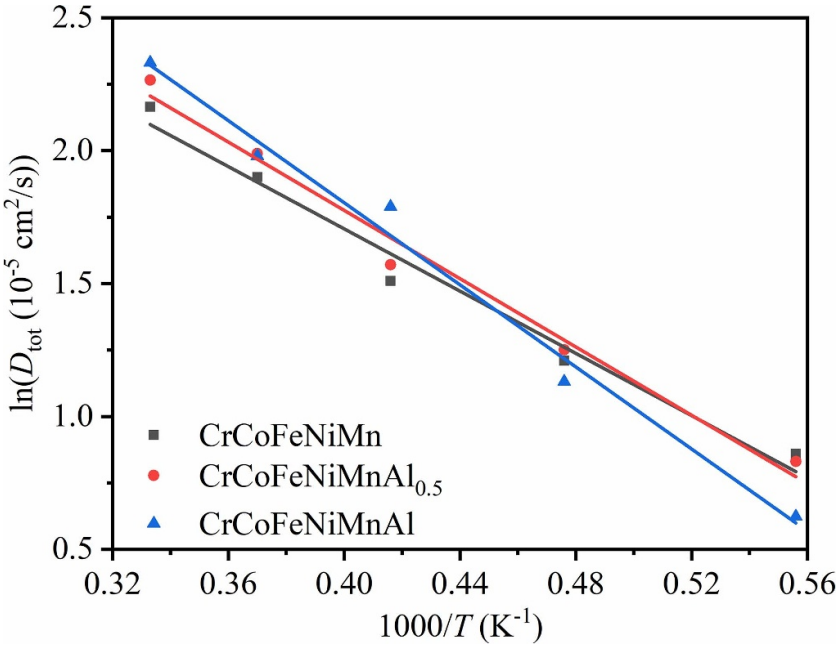

Figure 7. The variation in total self-diffusion coefficients of the three HEAs with temperature.

non-uniformity increases with the decrease of temperature, and the time required to reach the maximum non-uniformity also increases. In addition, the peak of $\chi_4(t)$ and the time to reach the peak of the three alloys gradually increases with the temperature decreasing from 3000 to 2100 K, but when the temperature drops to 1800 K, the peak and time increase sharply. This mutation means that the motion state of three HEAs melts changes from uniform at 2100 K to heterogeneity at 1800 K.

From above discussion, we know that the atom motion of the three HEAs are homogeneous from 3000 to 2100 K. To further analysis, the total self-diffusion coefficients D_{tot} within this temperature range are estimated from the slope of the MSD curve based on the Einstein relation,

$$D_\alpha = \lim_{t\to\infty} R_{i\alpha}^2(t)/6t \tag{6}$$

in which α is atom type and t is the time elapsed. The temperature-dependent D_{tot} is plotted in figure 9 and tested by Arrhenius formula,

$$D_\alpha = D_0 e^{-E_\alpha/RT} \tag{7}$$

in which E_α is the activation energy of α species, D_0 is the pre-exponential factor, and R is the gas constant. It can be clearly seen from figure 7 that the D_{tot} can be perfectly fitted by equation (7) with the values of R^2 about 0.97. Fitting ln$D$ and 1/T to a linear function, the activation energies E_α of CrCoFeNiMn, CrCoFeNiMnAl$_{0.5}$, and CrCoFeNiMnAl are achieved at 48.64, and 56.44, and 66.51 kJ mol^{-1}. Correspondingly, the pre-exponential factors D_0 are 0.58×10^{-3}, 0.93×10^{-3} and 1.48×10^{-3} cm^2 s^{-1}, respectively.

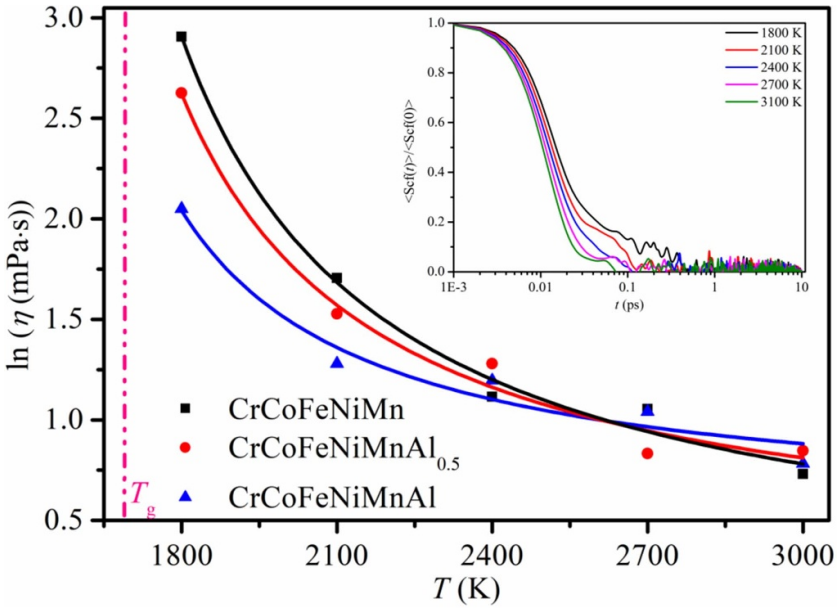

Figure 8. The variation of η with the temperature above temperature T_g. The inset shows the normalized shear auto-correlation function.

3.5. Structure-dynamic relation

To expound the structure-dynamic relationship, the shear viscosity of the three HEAs melts, another key transport property characterizing fluid kinetic, is obtained from the shear auto-correlation function [38],

$$\eta = \frac{V}{k_B T} \int_0^\infty \langle \sigma_{\alpha\beta}(t) \cdot \sigma_{\alpha\beta}(0)\, dt \rangle \tag{8}$$

where η is the shear viscosity of HEAs melt, V is the volume, k_B is the Boltzmann constant, and $\sigma_{\alpha\beta}(t)$ is the off-diagonal components of the stress tensor at time t. The shear auto-correlation function of CrCoFeNiMn from 3000 to 1800 K is depicted in the inset of figure 8.

The temperature dependence of shear viscosity above glass transition temperature T_g in the three HEAs melts is illustrated in figure 8. As the temperature approaches T_g, the shear viscosity rises dramatically and deviates from the Arrhenius function, which means the dynamic deceleration of the supercooled liquid. The extent to which viscosity reveals non-Arrhenius behavior is usually parameterized by fitting T and η to the Vogel–Fulcher–Tammann (VFT) formula, [37, 38]

$$\eta = \eta_0 \exp\left(\frac{D^* T_0}{T - T_0}\right) \tag{9}$$

in which η_0 is the viscosity at infinite liquidus temperature, T_0 is the temperature at which η becomes infinite, and D^* is an indicator of liquid fragility. The fitted T_0 is 1408 K for CrCoFeNiMn, 1419 K for $CrCoFeNiMnAl_{0.5}$, and 1432 K for CrCoFeNiMnAl. D^* is an appropriate parameter to characterize liquid, because with the increase of D^*, VFT moves closer to

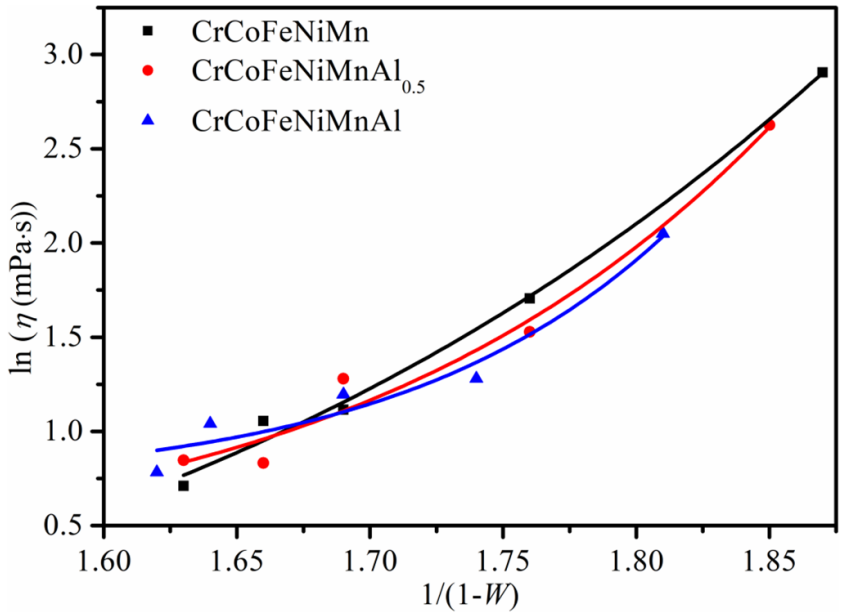

Figure 9. The viscosity η as a function of W.

Arrhenius function by degrees, which is consistent with stronger (less fragile) liquids. In this research, the fitted values of D^* are 0.78 for CrCoFeNiMn, 0.64 for CrCoFeNiMnAl$_{0.5}$, and 0.39 for CrCoFeNiMnAl, respectively. This suggests that the melt of HEAs becomes more brittle with the decrease in Al content. As previously reported, the more fragile the liquid, the weaker the GFA [38, 41]. This implies that the GFA of HEAs weakens with the addition of Al. Finally, in line with T_g, the T_0 of HEAs increases with the rise in Al content.

Combined with the diagram of the five-fold symmetry parameter, it can be found that the changing trend of W and η with temperature is consistently above T_g. Thus, it is speculated that the change in viscosity may be related to the underlying elementary structural evolution [37, 38, 42]. Besides that, we also find that the values of T_1 (1408, 1417, and 1434 K) for three HEAs are extremely close to T_0 (1409, 1419, and 1432 K). Therefore, by replacing T_0 in the VFT formula with T_1, the temperature variations can be removed, so that the direct relationship between W and η is obtained,

$$\eta = \eta_0 \exp\left(\frac{B}{(1-W)^{\delta}}\right) \tag{10}$$

in which δ is a parameter reflecting the sensitivity of viscosity changes to local structural changes. As illustrated in figure 9, the simulated data can be satisfactorily fitted by equation (10), and the statistical correlation parameters R^2 of the three HEAs are all greater than 0.93. As a result, the fitted values for δ are 6.70 for CrCoFeNiMn, 10.95 for CrCoFeNiMnAl$_{0.5}$, and 16.39 for CrCoFeNiMnAl, whereas the fitted B is found to be similar in the different HEAs, about 10^{-4}. The δ of the three HEAs is greater than 10, far more than 1, implying that small changes in structure will result in significant changes in viscosity. Since the higher the δ value, the greater the change of viscosity with W, the change in CrCoFeNiMnAl melt is more remarkable compared with other HEAs melts. In conclusion, structural evolution

is the basic driving factor of dynamic deceleration, and the 'hidden' structural changes leading to the extreme dynamic changes of the supercooled liquid can be clearly described by the structural parameter W.

4. Conclusions

AIMD simulations are implemented to investigate CrCoFeNiMnAl$_x$ ($x = 0$, 0.5, and 1) HEAs under a rapid solidification process. The trajectory of the system generated by the AIMD simulations is analyzed by a RDF, Voronoi tessellation, MSD, and shear auto-correlation function. These analytical methods reveal gradually the structural evolution and dynamical properties of CrCoFeNiMnAl$_x$ alloy under a constant cooling rate, 1.25×10^2 K ps^{-1}.

From the perspective of structural evolution, there are two conclusions. First, three HEAs all form metallic glass after rapid cooling, mainly composed of ICOS-like clusters and FCC-like clusters. The ratio of ICOS-like clusters to FCC-like clusters is affected greatly by Al content. At 300 K, the ratio is 4.52 for CrCoNiFeMn, 3.74 for CrCoNiFeMnAl$_{0.5}$, and 1.64 for CrCoNiFeMnAl, respectively. Second, the ideal glass transition temperatures (T_g) are predicted to be 1658 K for CrCoFeNiMn, 1667 K for CrCoFeNiMnAl$_{0.5}$, and 1687 K for CrCoFeNiMnAl, respectively. The T_g increasing with the Al content increasing.

From the perspective of dynamical properties, there are two conclusions. Firstly, the motion state of three HEAs melts changes from uniform at 2100 K to heterogeneity at 1800 K. Secondly, a relationship between structure and dynamics is established by using the five-fold local symmetry parameters and shear viscosity, which proves that the structural evolution is the fundamental reason of dynamic deceleration. The results provide a new perspective for studying the structural mechanism of dynamic retardation in HEAs.

Data availability statement

The data cannot be made publicly available upon publication because no suitable repository exists for hosting data in this field of study. The data that support the findings of this study are available upon reasonable request from the authors.

Acknowledgments

The authors gratefully acknowledge the financial support provided for Project Number 21ZR1435400 by the Science and Technology Commission of Shanghai Municipality. Z G acknowledges the support of the National Natural Science Foundation of China (Nos. 12104356, 52250191), China Postdoctoral Science Foundation (No. 2022M712552), the Opening Project of Shanghai Key Laboratory of Special Artificial Microstructure Materials and Technology (Ammt2022B-1), and the Fundamental Research Funds for the Central Universities. The computations in this paper were run on the Siyuan-1 cluster supported by the Center for High Performance Computing at Shanghai Jiaotong University. We also acknowledge the support by HPC Platform, Xi'an Jiaotong University.

ORCID iDs

Luyu Wang https://orcid.org/0000-0001-9671-6721
Zhibin Gao https://orcid.org/0000-0002-6843-381X

References

[1] Yeh J-W, Chen S-K, Lin S-J, Gan J-Y, Chin T-S, Shun T-T, Tsau C-H and Chang S-Y 2004 Nanostructured high-entropy alloys with multiple principal elements: novel alloy design concepts and outcomes *Adv. Eng. Mater.* **6** 299–303

[2] Cantor B, Chang I T H, Knoght P and Vincent A J B 2004 Microstructural development in equiatomic multicomponent alloys *Mater. Sci. Eng.* A **375–377** 213–8

[3] Li J, Meng X, Wan L and Huang Y 2021 Welding of high entropy alloys: progresses, challenges and perspectives *J. Manuf. Process.* **68** 293–331

[4] Zhang Y, Zhou Y J, Lin J P, Chen G and Liaw P 2008 Solid-solution phase formation rules for multi-component alloys *Adv. Eng. Mater.* **10** 534–8

[5] Arif Z U, Khalid M Y and Rehman E U 2022 Laser-aided additive manufacturing of high entropy alloys: processes, properties, and emerging applications *J. Manuf. Process.* **78** 131–71

[6] Wang W R, Wang W L, Wang S C, Tsai Y C, Lai C H and Yeh J W 2012 Effects of Al addition on the microstructure and mechanical property of Al_xCoCrFeNi high-entropy alloys *Intermetallics* **26** 44–51

[7] Zhao S, T, Li Z Z, ZHu C Y, Yang W, Zhang Z, Armstrong D E J, Grant P S, Ritchie R O and Meyers M A 2021 Amorphization in extreme deformation of the CrMnFeCoNi high-entropy alloy *Sci. Adv.* **5** eabb3108

[8] Inoue A 1995 High strength bulk amorphous alloys with low critical cooling rates (overview) *Mater. Trans. JIM* **36** 866–75

[9] He J Y, Liu W H, Wang H, Wu Y, Liu X J, Nieh T G and Lu Z P 2014 Effects of Al addition on structural evolution and tensile properties of the FeCoNiCrMn high-entropy alloy system *Acta Mater.* **62** 105–13

[10] Yang T F, Xia S Q, Wang C X, Wang C, Liu S, Zhang Y, Xue J, Yan S and Wang Y 2015 Effects of Al addition on microstructure and mechanical properties of AlxCoCrFeNi high-entropy alloy *Mater. Sci. Eng.* A **648** 15–22

[11] Bai L, Liu Y Z, Guo Y Y, Lv Y, Guo T and Chen J 2021 Effects of Al addition on microstructure and mechanical properties of Co-free $(Fe_{40}Mn_{40}Ni_{10}Cr_{10})_{100-x}Al_x$ high-entropy alloys *J. Alloy Compd.* **879** 160342

[12] Kresse G and Hafner J 1993 *Ab initio* molecular dynamics for liquid metals *Phys. Rev.* B **47** 558

[13] Kresse G and Furthmüller J 1996 Effifficient iterative schemes for *ab initio* total-energy calculations using a plane-wave basis set *Phys. Rev.* B **54** 11169

[14] Song J, Shi S P, Li X J and Yan L 2017 First-principle molecular dynamics modeling of UCl_3 in LiCl-KCl eutectic *J. Mol. Liq.* **234** 279–86

[15] Perdew J P, Burke K and Ernzerhof M 1996 Generalized gradient approximation made simple *Phys. Rev. Lett.* **77** 3865

[16] Perdew J P and Burke K 1996 Comparison shopping for a gradient-corrected density functional *Int. J. Quantum Chem.* **57** 309–19

[17] Blöchl P E 1994 Projector augmented-wave method *Phys. Rev.* B **50** 17953–79

[18] Kresse G and Joubert D 1999 From ultrasoft pseudopotentials to the projector augmented wave method *Phys. Rev.* B **59** 1758

[19] Song J, Wang L Y, Fan D, Zhang L, Wu W and Gao Z 2021 Cooling rate dependence of the properties for $Ti_{110}Al_{14}V_4$ alloy investigated by *ab initio* molecular dynamics *J. Mol. Liq.* **343** 117604

[20] Barman S, Gupta K K and Dey S 2024 Probing atomistic deformation behavior of graphene-coated $Al_{0.3}$CoCrFeNi high-entropy alloy under nanoindentation *J. Micromech. Mol. Phys.* 1–14

[21] Barman S, Gupta K K and Dey S 2024 Enhancing mechanical performance of $Al_{0.3}$CoCrFeNi HEA films through graphene coating: insights from nanoindentation and dislocation mechanism analysis *Model. Simul. Mater. Sci. Eng.* **32** 035012

[22] Han J J, Wang W Y, Liu X J, Wang C P, Hui X D and Liu Z K 2014 Effect of solute atoms on glass-forming ability for Fe-Y-B alloy: an *ab initio* molecular dynamics study *Acta Mater.* **77** 96–110

[23] Xu C-Q, Lee M-S, Wang Y-G, Cantu D C, Li J, Glezakou V-A and Rousseau R 2017 Structural rearrangement of Au-Pd nanoparticles under reaction conditions: an *ab initio* molecular dynamics study *ACS Nano* **11** 1649–58

[24] Li Y L, Xia W L, Qin J Y, Zhao D and Zuo M 2021 The special chemical short-range order and solidification behavior of Cu-Fe-P immiscible alloys *J. Mol. Liq.* **344** 117936

[25] Rajkumar V B, Du Y, Wang J and Liu Y 2020 Diffusivities of Cu-Ni and Cu-Si liquids calculated via ab initio molecular dynamics and the assessment of atomic mobilities *J. Mol. Liq.* **315** 112930

[26] Yu Q, Guo F M, Wang X D, Ståhl K, Ren Y, Cao Q P, Zhang D X and Jiang J Z 2019 Structural evolution of low-temperature liquid GaIn eutectic alloy *J. Mol. Liq.* **293** 111464
[27] Li R D, Niu P D, Yuan T C, Cao P, Chen C and Zhou K 2018 Selective laser melting of an equiatomic CoCrFeMnNi high-entropy alloy: processability, non-equilibrium microstructure and mechanical property *J. Alloys Compd.* **746** 125–34
[28] Cheng Y Q and Ma E 2011 Atomic-level structure and structure-property relationship in metallic glasses *Prog. Mater. Sci.* **56** 379–473
[29] Ding J, Asta M and Ritchie R O 2018 Melts of CrCoNi-based high-entropy alloys: atomic diffusion and electronic/atomic structure from *ab initio* simulation *Appl. Phys. Lett.* **113** 111902
[30] Jiang J, Sun W F and Luo N 2022 Molecular dynamics study of microscopic deformation mechanism and tensile properties in Al_xCoCrFeNi amorphous high-entropy alloys *Mater. Today Commun.* **31** 103861
[31] Li J, CHen H T, Li S X, Fang Q, Liu Y, Liang L, Wu H and Liaw P K 2019 Tuning the mechanical behavior of high-entropy alloys via controlling cooling rates *Mater. Sci. Eng.* A **760** 359–65
[32] Zhang Q, Wang J C, Tang S, Wang Y, Li J, Zhou W and Wang Z 2019 Molecular dynamics investigation of the local structure in iron melts and its role in crystal nucleation during rapid solidification *Phys. Chem. Chem. Phys.* **21** 4122
[33] Liu X J, Xu Y, Hui X, Lu Z P, Li F, Chen G L, Lu J and Liu C T 2010 Metallic liquids and glasses: atomic order and global packing *Phys. Rev. Lett.* **105** 155501
[34] Hirata A, Kang L J, Fujita T, Klumov B, Matsue K, Kotani M, Yavari A R and Chen M W 2013 Geometric frustration of icosahedron in metallic glasses *Science* **341** 376–9
[35] Sheng H W, Luo W K, Alamgir F M, Bai J M and Ma E 2006 Atomic packing and short-tomedium-range order in metallic glasses *Nature* **439** 419–25
[36] Celtek M 2022 An in-depth investigation of the microstructural evolution and dynamic properties of $Zr_{77}Rh_{23}$ metallic liquids and glasses: a molecular dynamics simulation study *J Appl. Phys.* **132** 035902
[37] Mauro N A, Blodgett M, Johnson M L, Vogt A J and Kelton K F 2014 A structural signature of liquid fragility *Nat. Commun.* **5** 4616
[38] Hu Y C, Li F X, Li M Z, Bai H Y and Wang W H 2015 Five-fold symmetry as indicator of dynamic arrest in metallic glass-forming liquids *Nat. Commun.* **6** 8310
[39] Parisi G and Sciortino F 2013 Structural glasses: flying to the bottom *Nat. Mater.* **12** 94–95
[40] Ediger M D 2000 Spatially heterogeneous dynamics in supercooled liquids *Annu. Rev. Phys. Chem.* **51** 99–128
[41] Angell C A 1995 Formation of glasses from liquids and biopolymers *Science* **267** 1924–35
[42] Watanabe K and Tanaka H 2008 Direct observation of medium-range crystalline order in granular liquids near the glass transition *Phys. Rev. Lett.* **100** 158002